Available online at www.sciencedirect.com
SCIENCE DIRECT®
Journal of Solid State Chemistry 177 (2004) 2168–2176
JOURNAL OF SOLID STATE CHEMISTRY
http://elsevier.com/locate/jssc

On the structure of the disordered $Bi_2Te_4O_{11}$ phase

O. Masson,[a,*] P. Thomas,[a] O. Durand,[a] T. Hansen,[b] J.C. Champarnaud,[a] and D. Mercurio[a]

[a] *Faculté des Sciences, Département de Chimie, Université de Limoges, Science des Procédés Céramiques et de Traitements de Surfaces UMR 6638 CNRS, 123 avenue Albert Thomas, 87060 Limoges Cedex, France*

[b] *Institut Laue-Langevin, 6, rue Jules Horowitz BP 156, 38042 Grenoble Cedex 9, France*

Received 4 November 2003; received in revised form 27 February 2004; accepted 3 March 2004

Abstract

The structure of the disordered metastable $Bi_2Te_4O_{11}$ phase has been investigated using both neutron powder diffraction and reverse Monte Carlo (RMC) modelling. The average structure, of fluorite-type (space group $Fm\bar{3}m$), is characterized by very high Debye-Waller parameters, especially for oxygen. Whereas the cations form a fairly well-defined FCC lattice, the oxygen sublattice is very disordered. It is shown that the local order is similar to that present in the stable monoclinic $Bi_2Te_4O_{11}$ phase. Clear differences are observed for the intermediate range order. The present phase is analogous to the "anti-glass" phases reported by Trömel in other tellurium-based mixed oxides. However, whereas Trömel defines anti-glass as having long range order but no short range order, it is shown here that this phase is best described as an intermediate state between the amorphous and crystalline states, i.e. having short and medium range order similar to that of tellurite glasses and a premise of long range order with the cations only.

Keywords: Disordered structure; Neutron diffraction; Reverse Monte Carlo modelling

1. Introduction

Bismuth tellurites are attractive materials from both fundamental and engineering applications points of view. This is partly due to the lone electron pairs of bismuth and tellurium atoms which are generally stereochemically active and which confer good non-linear optical properties on the materials. Among the bismuth tellurites, the $Bi_2Te_4O_{11}$ compound, although well studied, still raises questions; in particular concerning the structure of its cubic polymorph. It is known that the $Bi_2Te_4O_{11}$ compound has two polymorphs. The stable one (α-$Bi_2Te_4O_{11}$) was first studied by Frit et al. [1]. Its structure was completely determined by Rossel et al. [2]. It has a monoclinic symmetry (space group $P2_1/n$) and is related to the fluorite structure. More precisely, it is an anion-deficient superstructure of fluorite composed of an ordered intergrowth of $Bi_2Te_2O_7$ (fluorite-type) and Te_2O_4 (rutile-type) layers. The metastable polymorph (β-$Bi_2Te_4O_{11}$) was reported first by El Farissi [3] and later by Astaf'ev et al. [4]. It forms under fast crystallization of the $Bi_2Te_4O_{11}$ melt. Its structure and its phase transition toward the stable monoclinic form were recently investigated by Szaller et al. [5] and Lovas et al. [6] using X-ray powder diffraction and selected area electron diffraction. This phase is presented as having a nearly perfect oxygen-deficient fluorite-type structure ($Fm\bar{3}m(O_h^5)$, $a = 5.636$ Å, $Z = 4$) with no chemical ordering, i.e. tellurium and bismuth atoms evenly distributed on the cation sites. However, there is some inconsistency in describing the actual structure by the fluorite model. To our knowledge, there is no precedent of such crystal-chemistry of Te (IV). Indeed, a fluorite structure with a cell parameter of 5.636 Å requires Te–O bond lengths of about 2.44 Å which is much larger than the usual Te–O bond lengths found in other crystalline tellurites ($\sim$1.87–2.20 Å), and notably in the α-$Bi_2Te_4O_{11}$. In addition, each cation is coordinated by eight anions whereas in all-known tellurite, Te(IV) is commonly coordinated by three or four oxide ions. In the paper of Lovas et al. [6], no mention is made of the presence of atomic displacement disorder which could account for

*Corresponding author. Fax: +33-5-55-45-72-70.
E-mail address: olivier.masson@unilim.fr (O. Masson).

0022-4596/$ - see front matter © 2004 Elsevier Inc. All rights reserved.
doi:10.1016/j.jssc.2004.03.010

such a discrepancy. The isotropic displacement parameters they obtained by Rietveld refinements are indeed relatively low. In the same line of thought, the phase transition toward the stable form is described as a chemical ordering of the cations and the oxygen vacancies but no mention is made about the change in the short and medium range orders that a transition from a fluorite to the monoclinic structure would require.

The aim of the present paper is to clarify some of the aspects discussed above, in particular those concerning the actual nature of the metastable β-$Bi_2Te_4O_{11}$ phase. A first part is devoted to the study of the average structure by analyzing the Bragg scattering. This part already emphasizes important differences with respect to previous results. The second part deals with a more in-depth description of the actual structure by analyzing the total scattering. In particular, we discuss its relation to the monoclinic one, notably from the short and intermediate range orders point of view.

2. Experimental

2.1. Sample preparation

Polycrystalline samples of the $Bi_2Te_4O_{11}$ metastable compound were synthesized from a mixture of pure Bi_2O_3 and TeO_2 in stoichiometric (1:4) proportions. Starting materials were Bi_2O_3 (Aldrich 99.9%) and TeO_2 prepared from thermal decomposition of orthotelluric acid H_6TeO_6 (Aldrich 99.9%) at 550°C for 24 h. In order to prevent from oxidation of tellurium (IV) during synthesis, the sample was prepared in sealed gold tube. The oxides mixture was melted at 730°C for 1 h and quenched to room temperature in water. No change of weight occurred.

The measured density of the sample is $\rho_{exp} = 6.84(1)\,g/cm^3$ ($\rho_{th} = 6.83\,g/cm^3$). The metastable modification is thus less dense than the stable α-$Bi_2Te_4O_{11}$ phase ($\rho_{exp} = 7.10(4)\,g/cm^3$). Note also that this sample progressively transforms into the stable phase at temperatures above 450°C, as previously shown [5].

2.2. Measurement techniques

Because of the metastable nature of this phase, it was not possible to obtain large single-crystals, so that the subsequent structural analysis was performed on powder samples.

Preliminary measurements were done by X-ray diffraction. Patterns were collected at room temperature using Cu$K\alpha$ ($\lambda = 1.5418$ Å) radiation on a Siemens-Brüker D5000 Bragg-Brentano ($\theta-2\theta$) powder diffractometer with graphite secondary monochromator. The data were collected in the 8–125° 2θ range with a step size of 0.02° 2θ. The Rietveld analysis was performed with the FullProf [7] program.

Total neutron diffraction experiments were carried out on the D20 high flux diffractometer at the ILL (Institut Laue-Langevin). This reactor based instrument uses a curved position-sensitive detector which covers 153.6° 2θ and operates in a wide range of wavelengths. A wavelength of 0.7985 Å was used, enabling us to record intensities up to $Q_{max} = 15\,Å^{-1}$ ($Q = 4\pi \sin\theta/\lambda$). The powder samples were placed in a thin-walled (2.5 μm) vanadium container of 6 mm in diameter. The experiments were performed under vacuum, both at room and low (10 K) temperatures.

In order to extract the total static structure factor $S(Q)$, the neutron raw data were corrected (for zero and sample displacement errors, background artifacts, absorption, inelastic and multiple scattering) and normalized using the program CORRECT [8]. The total pair-correlation function $G(r)$ was derived from $S(Q)$ with the following integral equation:

$$S(Q) - 1 = \rho_0 \int 4\pi r^2 (G(r) - 1) \frac{\sin Qr}{Qr} \mathrm{d}r, \quad (1)$$

where ρ_0 is the atomic density of the sample. Inversion of Eq. (1) was achieved indirectly by using a Monte Carlo-based inversion method [9], which allows, in contrast to the conventional direct Fourier transform, to correctly handle noise, truncation of data and the finite resolution of the instrument.

2.3. RMC modelling

In simple systems, quantitative information about the local structure, e.g. the coordination numbers, can be directly obtained from the peak areas in the total pair-correlation function. Gaussian functions are for instance fitted to peaks which have been assigned to particular bonding pairs. For the three components system considered here, the total pair-correlation function contains six partial pair functions. This induces a high overlap of peaks and thus large uncertainties in the result.

For this reason, structural information was extracted using the Reverse Monte Carlo algorithm (RMC) [10]. In this method, experimental data from diffraction or other techniques are used to generate real space models of the sample. An initial model is randomly varied until the best agreement with both data and constraints on the structure is obtained. Constraints are essential to severely limit the number of structures that are consistent with the data. It is indeed well-established [11] that RMC methods do not produce a unique solution but instead a three-dimensional structure, generally the most disordered, which is simply consistent with the data and constraints.

Table 1
For each atom pair, the closest approach distance R_{min}, the maximum distance for calculating the coordination numbers R_{max}^{coord}, the maximum distance for calculating the bond valence sums R_{max}^{val} and the Faber-Ziman weighting coefficients used in the RMC model are given

Atom pair	R_{min} (Å)	R_{max}^{coord} (Å)	R_{max}^{val} (Å)	Neutron weight
Te–Te	3.08			0.04967
Te–O	1.68	2.44	3.1	0.27333
Te–Bi	3.16			0.07307
O–O	2.40			0.37602
Bi–O	2.08		3.1	0.20104
Bi–Bi	3.16			0.02687

Note that the R_{max}^{val} value has been chosen in order to get a contribution to the valence sum lower than 0.05.

In the present case, the RMC models were built with 2448 atoms (576 Te, 1584 O and 288 Bi) in a cubic box ($\sim$34 Å/side) at the proper density ($\rho_0 \sim 0.0633$ atom/Å^3). The RMC modelling of the total pair-correlation function and the total structure factor were achieved with the RMCA and RMCPOW [12] programs respectively. Constraints on the approach distances of the different atom pairs were applied using the minimum approach values reported in Table 1. These values are based on those found in other crystalline tellurites and mixed oxides, in particular in the monoclinic $Bi_2Te_4O_{11}$ phase. They are about 10% smaller than the corresponding distances found in other phases to allow disorder in the bond lengths. We modified the RMCA program in order to implement individual constraints on the coordination number and the bond valence sum of each atom type. These additional constraints enabled to generate the correct crystal-chemistry for tellurium, oxygen and bismuth atoms. The coordination number of tellurium atoms was constrained to 3 or 4, which corresponds to the usual TeO_3 or TeO_4 polyhedra found in tellurites. The coordination number of oxygen atoms was constrained to 1 or 2 to account for terminal or bridging oxygen. No constraint was applied for bismuth atoms as they can have quite variable coordination. Valence sums were constrained to 4 and 3 for tellurium and bismuth atoms respectively. The constraints have been implemented by adding for each constraint a term to the total χ^2 (i.e. the criterion minimized during RMC modelling) as follows:

$$\chi^2 = \cdots + \sum (1 - f_\alpha)^2 / \sigma^2,$$

where the sum is over all constraints, f_α is the proportion of atoms of type α that meet the required coordination number or bond valence sum and σ is a parameter weighting this constraint relatively to others and the fit to the data. Valence sums were calculated within the maximum distances reported in Table 1 using the exponential law and parameters from [13].

Also given in Table 1 are the Faber-Ziman weighing coefficients of the different partial structure factors. They show that neutron diffraction mainly probes the Te–O, Bi–O and O–O pair-correlations. Preferentially probing cation-cation pairs would require other kind of experiment (e.g. X-ray diffraction). In the present study, we are mainly interested in the cation–anion pair-correlation, the cation–cation pairs being largely constrained by the cationic long range order present in this phase.

3. Results and discussion

3.1. The average structure—Bragg scattering analysis

The X-ray powder diffraction pattern of the $Bi_2Te_4O_{11}$ sample is shown in Fig. 1. Only one crystalline phase is clearly present. The 15 diffraction lines in the 10–125° 2θ range can be unambiguously indexed in the $Fm\bar{3}m(O_h^5)$ cubic space group with $a = 5.636(4)$ Å, confirming previous results [5,6]. They do not exhibit significant extra broadening with respect to the instrument resolution, indicating that the structure has a fairly well-defined long range order. A Rietveld analysis was carried out with the chemically disordered fluorite structural model proposed by Lovas et al. [6] in which the 4*a* (000) position is filled with bismuth and tellurium atoms in 1/3–2/3 ratio and the 8*c* (1/4,1/4,1/4) positions are occupied by oxygen with 11/12 site occupancy. The fit is not perfect as attested by the residuals and the reliability factors. In addition, the isotropic displacement parameters are very large ($B_{Te} = B_{Bi} = 4.7$ Å^2, $B_O = 14.6$ Å^2), indicative of high displacement disorder, especially for oxygen. This result seems in contradiction

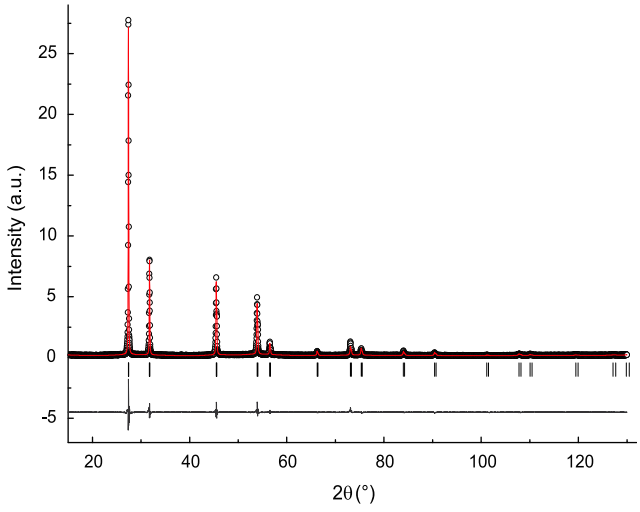

Fig. 1. Rietveld fit of the XRD powder pattern of the β-$Bi_2Te_4O_{11}$ sample. $R_p = 6.8\%$; $R_{wp} = 8.6\%$; $R_B = 3.4\%$; GoF = 1.4; DW (Durbin-Watson) = 1.2.

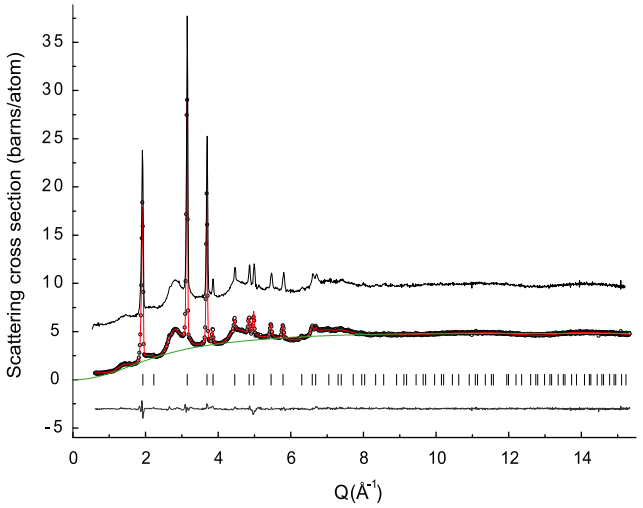

Fig. 2. Rietveld fit (the background signal is not fitted) of the neutron scattering cross-section for the β-$Bi_2Te_4O_{11}$ sample at room temperature $R_p = 1.08\%$; $R_{wp} = 1.56\%$; $R_B = 6.1\%$; GoF = 1.2; DW = 1.35. Diffuse scattering signal (dotted curve) calculated for uncorrelated Gaussian-distributed atom displacement and Rietveld refined B_{iso} values. Neutron scattering cross section for the β-$Bi_2Te_4O_{11}$ sample at 10 K (upper curve), shifted upward by 5 units for clarity.

with the relatively low oxygen displacement factor ($B_O = 4.8\,Å^2$) given by Lovas et al. [6], which suggests that the structure is well-ordered. However, we think that this low value is doubtful as only a very high B_O of about $15\,Å^2$ can account for the (222)/(200) line intensities ratio observed in the XRD pattern given in their paper.

The neutron structure factor is shown in Fig. 2. It contrasts with the XRD pattern. We can see diffraction lines of the fluorite lattice superimposed on a high background signal which increases rapidly with increasing Q to finally oscillate about a maximum at large Q values. The background signal is clearly associated with the oxygen atoms as the neutron coherent scattering lengths of the oxygen and tellurium atoms are almost identical (5.803 versus 5.8 b respectively), whereas for X-rays, the pattern is dominated by the scattering of tellurium (and bismuth). As shown below, it is associated with the displacement disorder of the oxygen atoms.

The Rietveld refinement of the neutron data obtained at room temperature gives basically the same results as with XRD data. In particular, it confirms the large displacement parameters of cations and oxygen atoms ($B_{Te} = B_{Bi} = 3.5\,Å^2$, $B_O = 18.3\,Å^2$). The fit is significantly improved with a split atom refinement in which tellurium, bismuth and oxygen atoms fill the 32*f* (*x*,*x*,*x*) position. The refined positions are $x = 0.035$ and 0.312 for Te/Bi and O atoms, respectively, and the isotropic displacement factors drop to $B_{Te} = B_{Bi} = 0.8\,Å^2$ and $B_O = 8.1\,Å^2$. Split atom refinements generally enable to take into account a non-Gaussian probability density function of the atom positions. Thus, the large displacement obtained for oxygen in the ⟨111⟩ directions indicates that whereas its average position is (1/4,1/4,1/4), few atoms are actually at this location but many are likely shifted toward the center of the cell or the middle of the edges.

The experiment carried out at 10 K gives almost the same results as for room temperature. As it can be seen from Fig. 2, differences in the diffraction pattern are indeed hardly noticeable with only a very small increase of the Bragg peaks intensities in the 5–7 $Å^{-1}$ Q range. It is thus very unlikely that the high oxygen Debye-Waller parameter be induced by thermal motions of atoms, so that the disorder present in this phase is certainly of static nature.

This oxygen displacement disorder induces diffuse scattering. For non-correlated atom displacement, distributed with a Gaussian probability density function, the coherent diffuse scattering can be approximated by [14]

$$I_{diff}^{coh}(Q) = \sum_k c_k |b_k|^2 (1 - \exp[-B_k Q^2 8\pi^2]), \quad (2)$$

where c_k, b_k and B_k are the concentration, the scattering length and the isotropic displacement factor of atomic species k in the system. By using the B_k′s obtained from the Rietveld refinement of the neutron data, we get the curve also depicted in Fig. 2. This curve scales and reproduces quite well the main trend of the experimental diffuse scattering, in particular the rapid increase with increasing Q. From a scattering point of view, the diffuse scattering is thus consistent with the decrease of the Bragg intensities. It is also obvious from Fig. 2 that the experimental diffuse scattering exhibits features that are not reproduced with Eq. (2). This indicates that the oxygen disorder is not fully random but exhibits local structural correlation.

3.2. The actual structure—total scattering analysis

To study the local structural correlation, one needs to consider the total structure factor, i.e. both Bragg and diffuse scattering. All this information is contained in the pair-correlation function.

The total pair-correlation function of the sample is shown in Fig. 3. There are 3 narrow peaks in the distance range from ~1.8 to ~3 Å and broad peaks further. Is also depicted for comparison the pair-correlation function of the monoclinic phase obtained with isotropic displacement parameters of $0.5\,Å^2$ for all atoms. One can immediately notice the strong analogy, especially in the low correlation length region, indicating that the local order of both phases is similar. The first and highest peak at ~1.90 Å is unambiguously assigned to the Te–O correlation lengths whereas the second peak at ~2.35 Å corresponds mainly to the Bi–O bond

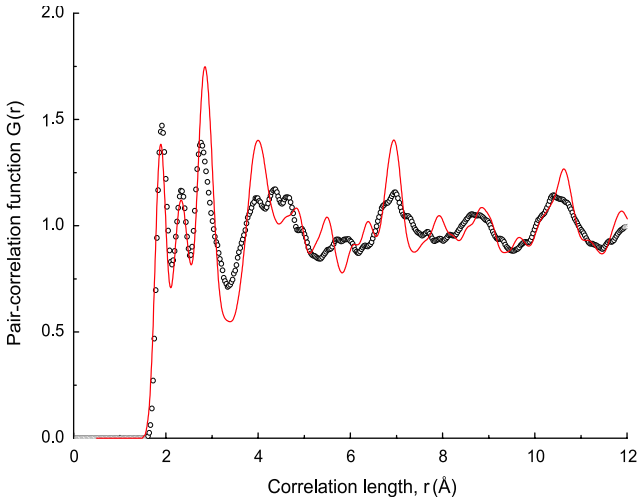

Fig. 3. Total pair-correlation function $G(r)$ from neutron diffraction measurement for the β-$Bi_2Te_4O_{11}$ sample (open circles) and for the α-$Bi_2Te_4O_{11}$ phase.

lengths. These preliminary results show that the actual structure has the typical Te–O bond lengths found in other crystalline tellurites, and not the 2.44 Å as expected with the fluorite model. Further information has to be extracted via RMC modelling.

3.2.1. The RMC model

In glass structure modelling, the initial configuration generally consists of a random arrangement of atoms within a cubic cell, with constraints on the density, the closest atomic approaches and the coordination numbers. In the present case, although highly disordered, the phase also exhibits long range order so that the χ^2 function has numerous deep local minima, which can rather complicate its minimization. A better initial configuration can be obtained by using a crystalline model. The fluorite phase with randomly disordered bismuth, tellurium atoms and oxygen vacancies has two main drawbacks. First, as stated above, its local order is very different from that present in the β-$Bi_2Te_4O_{11}$ phase, so that no coordination and valence constraints are met. Second, it is not easy to control how tellurium, bismuth atoms and oxygen vacancies are distributed or similarly to account for some correlations in the position of bismuth atoms and oxygen vacancies. Random does not mean uniform and it is likely that the initial model contains non-realistic clusters of bismuth atoms and oxygen vacancies. The starting model we used instead derives from the monoclinic phase, the underlying ideas being the followings: first, the short range order of the two phases is similar as discussed above, so that the chemistry of both tellurium and bismuth are satisfied in the starting model. Second, this phase has a fluorite sublattice, although distorted and chemically ordered, so that a slight modification can allow to get a good guess of the FCC cationic lattice of the disordered phase.

The relationship of this fluorite subcell (subscript F) to the monoclinic cell (subscript M) is:

$$\begin{pmatrix} a_F \\ b_F \\ c_F \end{pmatrix} = \frac{1}{6}\begin{pmatrix} -4 & 0 & 1 \\ 2 & -3 & 1 \\ 2 & 3 & 1 \end{pmatrix}\begin{pmatrix} a_M \\ b_M \\ c_M \end{pmatrix}.$$

The initial model was then obtained by first generating a large monoclinic structural block with slightly modified cell parameters $a = 6.9028$, $b = 7.9706$, $c = 19.524$ Å and $\alpha = \beta = \gamma = 90°$ (monoclinic cell parameters: $a = 6.9909(3)$, $b = 7.9593(3)$, $c = 18.8963(8)$ Å, $\alpha = \gamma = 90°$ and $\beta = 95.176(3)°$) in order to get non-distorted fluorite subcells with the proper cell parameter ($a = 5.636$ Å). A cubic box consisting of $6 \times 6 \times 6$ fluorite subcells was then extracted and origin was chosen to have bismuth and tellurium atoms located at the cube origin. The chosen $6 \times 6 \times 6$ size (~ 34 Å/side) is adequate for RMC modelling and enables to match the periodicity of the monoclinic phase. Next, the Te/Bi long range order corresponding to that of the monoclinic phase was partially destroyed by rotating a quarter or half a turn layers composed of 9 ($3 \times 3 \times 1$) cubic elements (each cubic element being composed of $2 \times 2 \times 2$ fluorite subcells) about the x, y and z axis in a sequential and random fashion (i.e. in the way used with the Rubik's cube game). Note that different sequences were used with no effect on the final result. Few atoms were finally moved out in such a way that the model fulfils the closest approach conditions.

The as-obtained model partly matches the local order of the monoclinic phase and a chemically disordered FCC cationic lattice. As one can see from Fig. 4, total neutron scattering calculated from this model agrees quite well with the experimental data even prior to RMC fitting. The main features of the pattern are indeed reproduced. This initial configuration is likely a simple and consistent description of the real structure even if it is obvious, from the difference in Bragg and diffuse intensities, that it is still too much ordered.

The RMC fit of both the total pair-correlation function in the range 0–17 Å and the total structure factor are shown in Fig. 4. The fit are satisfactory (although not perfect) with coordination constraints satisfied at 92% and 91% for tellurium and oxygen atoms respectively, valence constraints satisfied at 90% and 92% for tellurium and bismuth atoms with an average valence sum of 3.9 for tellurium atoms and 2.9 for bismuth atoms. This indicates that the assumptions made in the RMC model, i.e. the presence of interconnected TeO_3 or TeO_4 structural units as those usually found in crystalline tellurites, are consistent with the data. Some differences between the RMC fit

and the experimental total structure factor can be noticed in the lower Q region. A short range order peak at $Q \sim 1.4\,\text{Å}^{-1}$ corresponding to correlation length of $\sim 4.5\,\text{Å}$ in the structure is for example not reproduced by the model. These subtle differences are not well explained until now.

The projection of the model along the c-axis and its average structure, i.e. the projection of all unit cells into a single one, are given in Fig. 5. The projection of the monoclinic structure is also depicted for comparison. These pictures catch some of the main characteristics of the β-$Bi_2Te_4O_{11}$ phase, namely its disordered nature, its relation to the fluorite structure and its analogy with the monoclinic phase. In particular, the latter has also a large apparent displacement of the oxygen atoms with respect to the fluorite tetrahedral sites. This is necessary to account for the chemistry of tellurium and bismuth atoms given that cations form a fairly well-defined FCC sublattice. The slight distortion of this FCC sublattice can be interpreted as due to the Bi/Te ordering along a cubic $[111]_F$ direction in one set of $\{111\}_F$ planes.

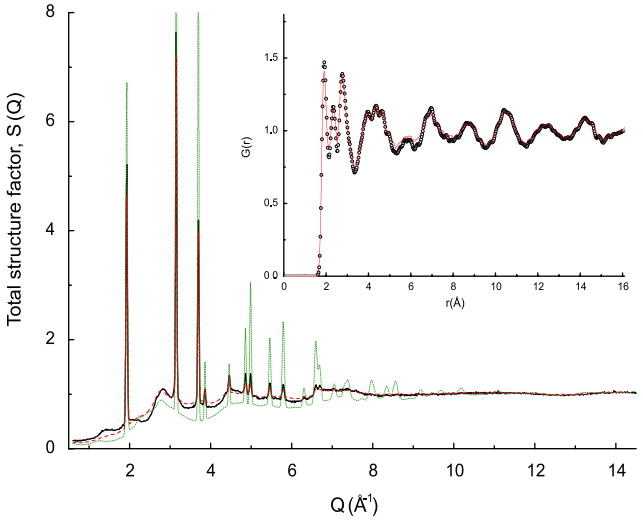

Fig. 4. Total neutron structure factor $S(Q)$ for the β-$Bi_2Te_4O_{11}$ phase : experimental (solid line), RMC fit (dashed line) and calculated from the initial (i.e. prior to RMC fit) RMC model (short dotted line). Inset: total pair distribution function $G(r)$ from neutron diffraction (open circles) and RMC fit (solid line).

3.2.2. *The short and intermediate range orders*

The partial pair-correlation functions obtained from the RMC model are depicted in Fig. 6. The cation–cation coordination shells corresponding to a FCC lattice are fairly well resolved. The peaks are relatively broad with almost the same width, indicative of an uncorrelated displacement disorder. In contrast, the O–O correlation function only exhibits one single peak at $\sim 2.8\,\text{Å}$ which correspond to the usual O–O distances found in the TeO_3 or TeO_4 polyhedra. Further, the correlation function is almost flat, indicating that the oxide sublattice is nearly completely disordered (neither medium nor long range order) similarly to what is found in tellurite glasses. The Te–O correlation function has an intense and very sharp maximum at $\sim 1.9\,\text{Å}$, a weaker maximum at $\sim 2.9\,\text{Å}$, and a much broader at $\sim 4.5\,\text{Å}$. The next coordination shells are barely resolved. The sharpness of the first peak indicates that there is no significant disorder in the Te–O bond lengths. Similar features are obtained with the Bi–O pair but with a slightly broader first peak at $\sim 2.4\,\text{Å}$. The proportion of TeO_3 is almost the same as that of TeO_4 for a cut-off radius of $2.4\,\text{Å}$. However, it seems that there is no clear boundary between TeO_3 and TeO_4 units as the

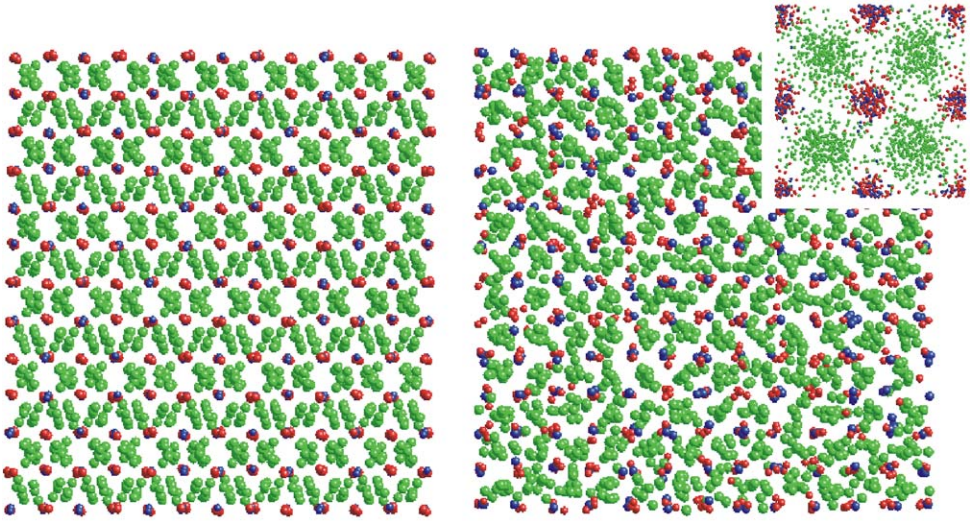

Fig. 5. Projection along the fluorite c-axis of the α-$Bi_2Te_4O_{11}$ phase (left), the β-$Bi_2Te_4O_{11}$ RMC model (right) and its average structure (upper right corner).

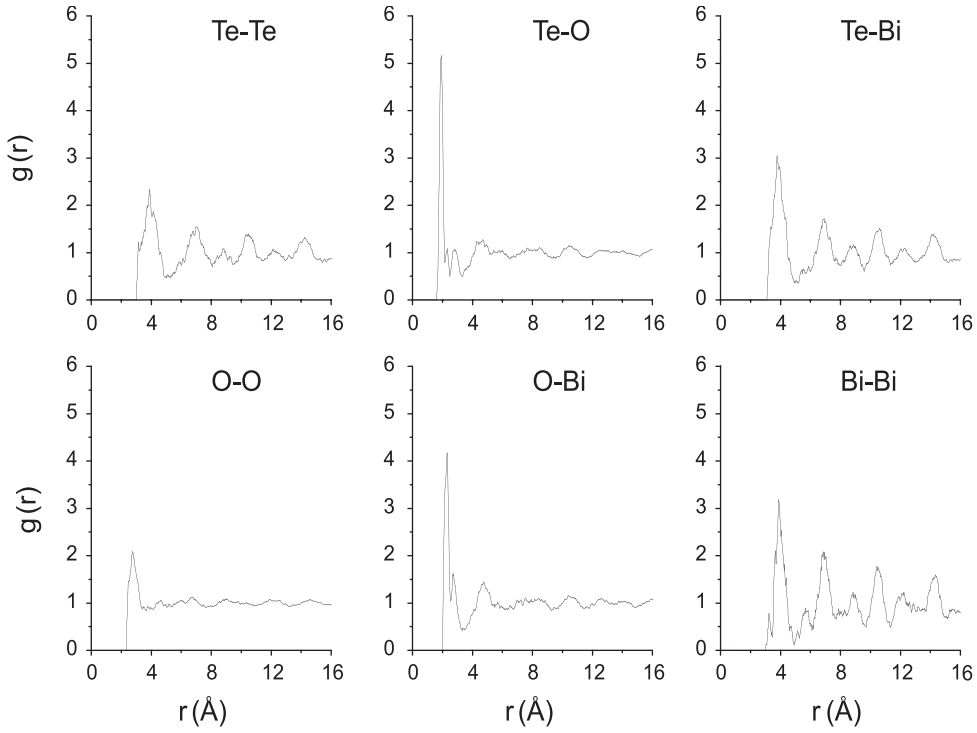

Fig. 6. Partial pair-correlation functions from the β-$Bi_2Te_4O_{11}$ RMC model.

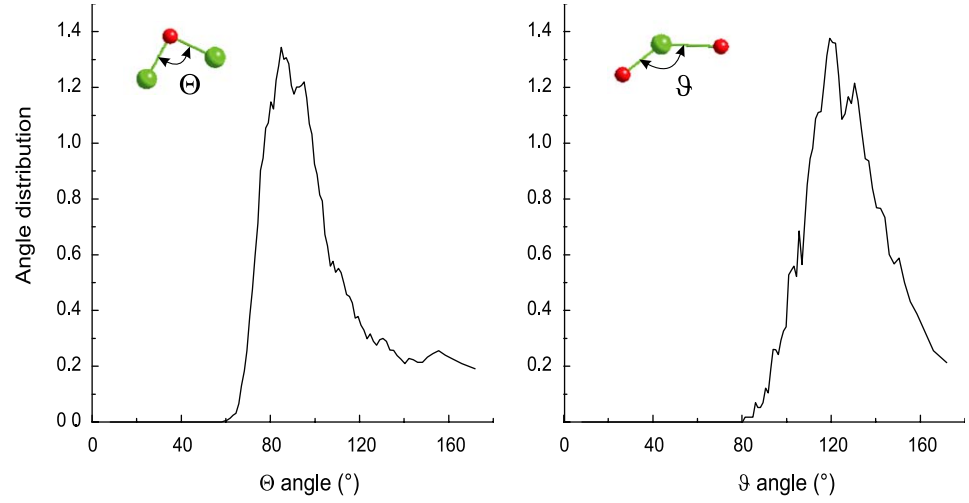

Fig. 7. O–Te–O (left) and Te–O–Te (right) bond angle distributions.

proportion depends slightly on the chosen cut-off radius. This contrasts with the monoclinic phase in which the local tellurium environment is clearly made of TeO_3 and TeO_4 in the 3:1 ratio. For bismuth atoms, the obtained coordination numbers are 8, 7 and 6 in the 20%, 50% and 22% proportions, respectively, and a small amount of less-realistic coordination numbers (<6). For the α-$Bi_2Te_4O_{11}$ phase, bismuth atoms are 7 or 8-fold coordinated in the same amount.

The O–Te–O and Te–O–Te bond angle distributions are given in Fig. 7. They are characterized by broad peaks, indicating that disorder affects mainly the bond valence angles. For the O–Te–O distribution, the peaks occur close to the internal angles of the TeO_3 and TeO_4 polyhedra found in the monoclinic phase and in pure tellurite polymorphs: for TeO_3 units, the angles lie between 85° and 100° and for TeO_4 units, bond angles are $\sim$96° for the equatorial oxygen and $\sim$178° for the axial one.

Concerning the Te–O–Te angle distribution, the peak is close to 120° and is clearly smaller than the 140–144° values found in the monoclinic phase. The Te–O–Te

angle distribution is characteristic of how the TeO_3 and TeO_4 polyhedra are linked together. It is thus indicative of the intermediate range order in the structure. As one can see in Fig. 8, the structure of the monoclinic phase can be described as an ordered sequence of tellurium-only layer and a mixed double layer containing equal numbers of bismuth and tellurium atoms (of composition $Bi_2Te_2O_7$). The composite double layer contains only isolated TeO_3 units. In the tellurium-only layers, TeO_3 and TeO_4 units are linked together by a single oxygen bridge to form parallel infinite long sinusoidal

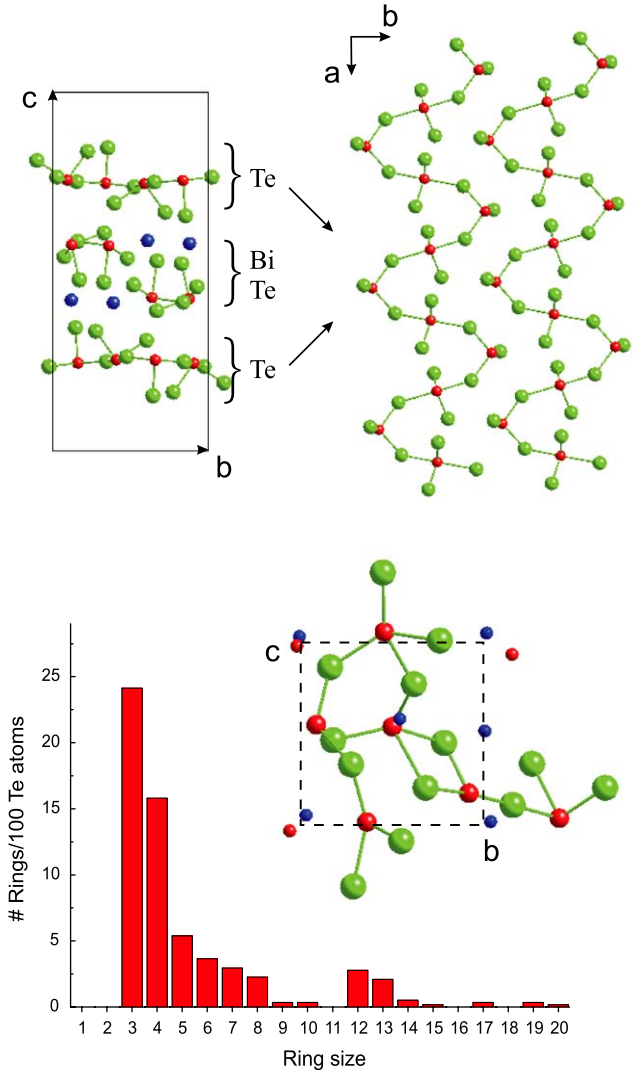

Fig. 8. Up: Typical features of the α-$Bi_2Te_4O_{11}$ structure: alternate sequence of tellurium-only and Bi/Te mixed layers. The composite double layer contains only isolated TeO_3 units and the tellurium-only layers are formed of parallel infinite long sinusoidal chains of TeO_3 and TeO_4 units linked together by a single oxygen bridge. Bottom: typical features of the β-$Bi_2Te_4O_{11}$ RMC model: projection along the c-axis of a single (distorted) FCC unit cell showing a part of a Te–O chain containing a 3-fold tellurium ring and a double oxygen bridge (the isolated smaller atoms are the other Te and Bi atoms of the FCC unit cell which are not involved in this chain). Also given is the tellurium rings distribution.

chains. Identical chains are present in the paratellurite α-TeO_2 phase [15]. In these chains, the Te–O–Te angles lie between 140° and 144°. The lower value found with the RMC model suggests that these sinusoidal chains do not form in the β-$Bi_2Te_4O_{11}$ phase. This could indicate that these chains can only form in tellurium-only layers, i.e. in the paratellurite α-TeO_2 phase or in the α-$Bi_2Te_4O_{11}$ phase. The bond angle found in the present case are rather indicative of other type of linkage as for instance the zigzag chains found in the γ-TeO_2 phase [16] or the double oxygen bridge present in the tellurite β-TeO_2 phase [17]. A close inspection of the structure of the RMC model reveals that there are mainly long cooked and branched chains, rings and few double oxygen bridges. Rings are interesting features as they are usually found in tellurite glasses, for example in sodium tellurite glasses [18] but not in the α-$Bi_2Te_4O_{11}$ phase. The ring distribution found in the model is given in Fig. 8. The maximum populated are the smallest, i.e. three-fold, rings. Are also present 4-, 5-, 6-membered and larger rings with a decreasing population. In many respects, the Te–O polyhedra linkage found in this phase seems closer to those found in tellurite glasses than those found in the α-$Bi_2Te_4O_{11}$ phase. This clear difference of intermediate range order with respect to the monoclinic phase may partly explain the relative stability of the β-$Bi_2Te_4O_{11}$ phase with respect to its transformation toward the α-$Bi_2Te_4O_{11}$ phase. A very substantial rearrangement is indeed required to break the small rings and generate long sinusoidal chains.

4. Concluding remarks

To conclude, whereas the β-$Bi_2Te_4O_{11}$ phase exhibits a fluorite-type average structure with quite well-defined long range order, it is shown that only the cations form a crystalline (FCC) lattice. The anions exhibit a large displacement disorder with respect to the tetrahedral sites in order to fulfil the crystal-chemistry of both bismuth and tellurium atoms. It is worth noting that similar phases have been observed in other chemical tellurium-oxide-based systems by Trömel [19]. Even if no structural details were given, their XRD pattern are typical of the fluorite structure and their Raman spectra are similar to that of tellurite glasses (the same kind of Raman spectra has been obtained for the present phase but it is not presented in this paper). These phases have been denominated by Tromel "antiglass" phases in order to account for what he defines as structure having long-range order but no short-range order. According to the present study, it appears that these phase are certainly best described as being an intermediate state between the glass and crystalline states in which the short range order is present and the cationic network has already formed as the premise of crystallization.

This phase is certainly a first stage of the crystallization of the stable α-$Bi_2Te_4O_{11}$ phase.

Acknowledgments

We would like to acknowledge the ILL staff for experimental support. One of us, O. Durand, is grateful to the Conseil Régional du Limousin for financial support. The authors would also like to acknowledge Prof. B. Frit for fruitful and stimulating discussions on the present work.

References

[1] B. Frit, M. Jaymes, Rev. Chim. Miner. 5 (1972) 837.
[2] H.J. Rossel, M. Leblanc, G. Férey, D.J.M. Bevan, D.J. Simpson, M.R. Taylor, Aust. J. Chem. 45 (1992) 1415.
[3] M. El Farissi, Thesis of the University of Limoges, 1987.
[4] S.A. Astaf'ev, A.A. Abdullaev, V.A. Dolgikh, B.A. Popovkin, Izu. Akad. Nauk SSSR Neorg. Mater. 5 (1989) 870.
[5] Zs. Szaller, L. Pöppl, Gy. Lovas, I. Dodóny, J. Solid State Chem. 121 (1996) 251.
[6] A. Lovas, I. Dodóny, L. Pöppl, Zs. Szaller, J. Solid State Chem. 135 (1998) 175.
[7] J. Rodriguez-Carvajal, FULLPROF program, See www-llb.cea.fr/fullweb/fp2k/fp2k.htm
[8] M.A. Howe, R.L. McGreevy, P. Zetterström, CORRECT program, See ftp://studsvik.uu.se/pub
[9] M.A. Howe, R.L. McGreevy, L. Pusztai, MCGR program, See ftp://studsvik.uu.se/pub
[10] R.L. McGreevy, L. Pusztai, Mol. Simul. 1 (1988) 359.
[11] R.L. McGreevy, P. Zetterström, J. Non-Cryst. Solids 293–295 (2001) 297.
[12] R.L. McGreevy, A. Mellegård, See ftp://studsvik.uu.se/pub
[13] N.E. Brese, M. O'Keeffe, Acta Crystallogr. B 47 (1991) 192.
[14] B.E. Warren, X-ray Diffraction, Addison-Wesley, Reading, MA, 1969.
[15] P.A. Thomas, J. Phys. C: Solid State Phys. 21 (1988) 4611.
[16] J.C. Champarnaud, S. Blanchandin, P. Thomas, A. Mirgorodsky, T. Merle, B. Frit, J. Phys. Chem. Solids 61 (2000) 1499.
[17] V.H. Beyer, Z. Kristallogr. 124 (1967) 228.
[18] J.C. McLaughlin, S.L. Tagg, J.W. Zwanzinger, D.R. Haeffner, S.D. Shastri, J. Non-Cryst. Solids 274 (2001) 1.
[19] M. Trömel, Z. Kristallogr. 183 (1988) 15.